Journal of Solid State Chemistry 183 (2010) 1992–1997

Contents lists available at ScienceDirect

Journal of Solid State Chemistry

journal homepage: www.elsevier.com/locate/jssc

$p(O_2)$-stability of $LaFe_{1-x}Ni_xO_{3-\delta}$ solid solutions at 1100 °C

E.A. Kiselev*, V.A. Cherepanov

Department of Chemistry, Ural State University, Lenin Ave. 51, 620083 Ekaterinburg, Russia

ARTICLE INFO

Article history:
Received 11 January 2010
Received in revised form
11 May 2010
Accepted 20 June 2010
Available online 1 July 2010

Keywords:
Perovskite
$LaFe_{1-x}Ni_xO_{3-\delta}$
Thermodynamic stability
Phase diagram

ABSTRACT

$LaFe_{1-x}Ni_xO_{3-\delta}$ ($x=0.1-1.0$) perovskites were synthesized via citrate route. The $p(O_2)$-stability of the perovskite phases $LaFe_{1-x}Ni_xO_{3-\delta}$ has been evaluated at 1100 °C based on the results of XRD analysis of powder samples annealed at various $p(O_2)$ and quenched to room temperature. The isothermal $LaFeO_{3-\delta}$–"$LaNiO_{3-\delta}$" cross-section of the phase diagram of the La–Fe–Ni–O system has been proposed in the range of oxygen partial pressure $-15 < \log p(O_2)/\text{atm} \le 0.68$. The unit cell parameters of orthorhombic perovskites *O*-$LaFe_{1-x}Ni_xO_{3-\delta}$ increase with decrease in $p(O_2)$ at fixed composition x. This behavior is explained on the basis of size factor. The decomposition temperatures of rhombohedral phases *R*-$LaFe_{1-x}Ni_xO_{3-\delta}$ for $x=0.7$, 0.8, 0.9 and 1.0 in air were determined as 1137, 1086, 1060 and 995 °C, respectively.

1. Introduction

Nonstoichiometric complex oxides of general formula $LaFe_{1-x}Ni_xO_{3-\delta}$, formed in the quasi-binary $LaFeO_{3-\delta}$–$LaNiO_{3-\delta}$ system, were suggested as promising materials for catalysis application and solid oxide fuel cell electrodes [1–11]. Recently, it was shown that $LaFe_{1-x}Ni_xO_{3-\delta}$ solid solutions could be considered as potential thermoelectric materials in thermoelectric generators for waste heat recycling [12,13].

The phase relations in the $LaFeO_{3-\delta}$–$LaNiO_{3-\delta}$ system in air were discussed earlier in [1,9,14–17]. Single-phase $LaFe_{1-x}Ni_xO_{3-\delta}$ solid solutions were found to crystallize in two different symmetries: orthorhombic symmetry (sp.gr. *Pbnm* or *Pnma*) or rhombohedral symmetry (sp.gr. $R-3c$), which define a crystal structure of the parent binary oxides $LaFeO_{3-\delta}$ or $LaNiO_{3-\delta}$, respectively. Lanthanum orthoferrite ($LaFeO_3$) is stable in air up to its melting point (~1900 °C) [18], while the thermal stability of lanthanum nickelate ($LaNiO_{3-\delta}$) is limited to 980–1000 °C [19,20]. Incorporation of iron into the nickel sublattice in $LaNiO_{3-\delta}$ increases its thermal stability [14,16]. However, the decomposition temperatures of $LaFe_{1-x}Ni_xO_{3-\delta}$ solid solutions have not been determined yet.

High-temperature XRD and dilatometry studies of $LaFe_{1-x}Ni_xO_{3-\delta}$ revealed the first-order phase transition from orthorhombic to rhombohedral structure [9]. The temperature of this phase transition decreased while nickel concentration (x) in $LaFe_{1-x}Ni_xO_{3-\delta}$ solid solutions increased and for compositions with $x=0.2$, $x=0.4$ and $x=0.5$ its value was about 650, 250 and 237 °C, respectively [9,17]. Available literature data on solubility limits (x) and crystal symmetry of $LaFe_{1-x}Ni_xO_{3-\delta}$ solid solutions is summarized in Table 1.

Phase equilibria and crystal structure of phases in the La–Fe–Ni–O system at 1100 °C in air were presented in our recent work [21]. It was shown that under these conditions, together with perovskite-type complex oxide series $LaFe_{1-x}Ni_xO_{3-\delta}$, the following solid solutions were formed: $La_4(Ni_{1-y}Fe_y)_3O_{10-\delta}$ ($0 \le y \le 0.3$), $La_3(Ni_{1-z}Fe_z)_2O_{7-\delta}$ ($0 \le z \le 0.05$), $La_2Ni_{1-v}Fe_vO_4$ ($0 \le v \le 0.05$), $Ni_kFe_{3-k}O_4$ ($0.81 \le k \le 1.05$), $Ni_{1-m}Fe_mO$ ($0 \le m \le 0.05$) and $Fe_{2-p}Ni_pO_3$ ($0 \le p \le 0.04$) [21]. However, there is no information about thermodynamic stability of the $LaFe_{1-x}Ni_xO_{3-\delta}$ oxides depending on oxygen partial pressure variations.

Thus, the aims of the present study are: (i) determination of the perovskite phase stability in the quasi-binary system $LaFeO_{3-\delta}$-"$LaNiO_{3-\delta}$" as a function of oxygen partial pressure at 1100 °C and (ii) evaluation of decomposition temperatures of the rhombohedral phases $LaFe_{1-x}Ni_xO_{3-\delta}$ with $x=0.7$, 0.8, 0.9 and 1.0 in air.

2. Experimental

The samples were synthesized via citrate precursor route. Chemically pure grade lanthanum nitrate hexahydrate $La(NO_3)_3 \cdot 6H_2O$, iron oxalate dihydrate $Fe(C_2O_4) \cdot 2H_2O$ and nickel acetate tetrahydrate $Ni(CH_3COO)_2 \cdot 4H_2O$ were used as starting materials. Stoichiometric amounts of the reagents were dissolved in the diluted nitric acid HNO_3 (1 vol of 65% acid to 3 vol of distilled water) to transform the corresponding oxalates and acetates into nitrates. After that an appropriate amount of citric acid monohydrate $C_6H_5O_4(OH)_3 \cdot H_2O$ (analytical-pure grade) was

* Corresponding author. Fax: +7 343 2615978.
E-mail addresses: Eugene.Kiselyov@usu.ru, evgenykiselev@e1.ru (E.A. Kiselev).

0022-4596/$ - see front matter © 2010 Elsevier Inc. All rights reserved.
doi:10.1016/j.jssc.2010.06.013

Table 1
Solubility limits (x) and symmetry of the $LaFe_{1-x}Ni_xO_{3-\delta}$ solid solutions. *O* – orthorhombic symmetry, *R* – rhombohedral symmetry.

Synthesis condition	Symmetry			Ref.
	O	*O*+*R*	*R*	
conventional solid state synthesis, pellets, 1250 °C	$0 \le x \le 0.5$	–	$x=0.6$	[1]
citric precursor, powder, 900 °C	$0 \le x \le 0.4$	$x=0.5$	$0.6 \le x \le 1$	[14]
nitrate precursor, pellets, 1450–1510 °C, slow cooled	$0.4 \le x \le 0.5$	–	$x=0.3$	[15]
citric precursor, powder, 1100 °C, quenched	$0 \le x \le 0.4$	$x=0.5$	$0.6 \le x \le 0.8$	[16]
citric precursor, pellets, 1000–1200 °C	$0 \le x \le 0.4$ (20 °C) $x=0.5$ (−243 °C)	$x=0.5$ (2–37 °C)	$x=0.2$ (800 °C) $x=0.4$ (600 °C) $x=0.5$ (127 °C)	[9,17]

added in order to substitute all nitrate groups to citrate. Slow heating of the citrate gel precursors led to formation of viscous gel, which during further increase of temperature dried and ignited spontaneously. Following heat treatment at 800 °C for 5 days with intermediate grindings allowed obtaining final products. The samples with composition $x=0.7$, 0.8, 0.9 and 1.0 were divided into two parts and treated in different ways.

The first part was used for electrical conductivity measurements in order to determine the thermal stability of $LaFe_{1-x}Ni_xO_{3-\delta}$ solid solutions in air. The samples for electrical conductivity measurements were prepared as follows. Obtained black fine powders of $LaFe_{1-x}Ni_xO_{3-\delta}$ with $x=0.7$, 0.8, 0.9 and 1.0 synthesized via decomposition of citrate precursors were pressed into rectangular bars under the pressure 15 MPa and finally sintered in air correspondingly at 1100, 1030, 900 and 850 °C for 12 h. XRD analysis of the samples, prepared in such a way, confirmed the presence of single rhombohedrally distorted perovskite phase (sp.gr. $R-3c$).

The samples for determination of phase equilibria at 1100 °C as a function of oxygen partial pressure were treated as follows. Prior to being annealed and quenched under various oxygen partial pressures at 1100 °C obtained powders of $LaFe_{1-x}Ni_xO_{3-\delta}$ with nominal compositions $x=0.1$, 0.2, 0.3, 0.4, 0.5, 0.6, 0.7, 0.8 and 0.9 were equilibrated at 1100 °C in air for 5 days with intermediate grindings every 20 h.

Phase composition and crystal structure of the samples were examined by XRD analysis using DRON4 diffractometer (Cu-$K\alpha$ radiation, Ni-filter, $2\theta=20$–70°, scan step$=0.02^\circ$). The XRD data were analyzed by means of the Rietveld method using FullProf package [22].

Phase equilibria and thermodynamic stability of the perovskite phases $LaFe_{1-x}Ni_xO_{3-\delta}$ in the $LaFeO_{3-\delta}$–"$LaNiO_{3-\delta}$" system were studied based on the results of XRD data for quenched samples. The powder samples were quenched from 1100 °C to room temperature in the leak-proof cell equipped with an electrochemical oxygen pump and a sensor in order to control the oxygen partial pressure. The samples of $LaFe_{1-x}Ni_xO_{3-\delta}$ were kept in alumina crucibles at a given oxygen partial pressure and temperature 1100 °C for 16–20 h to equilibrate them with an ambient atmosphere prior to quenching. Such anneals with following quenching to room temperature at required oxygen pressure were repeated several times until a uniformity between the previous and following XRD patterns had been achieved.

Decomposition temperatures for Ni-rich solid solutions ($x=0.7$, 0.8, 0.9 and 1.0) were determined in air by measuring their electrical conductivity at constant heating rate of 10°/h using a standard DC 4-probe technique.

Since the conductivity measurements were used only for the aim of thermal analysis, the densities of sintered samples had not been determined, though due to the relatively low sintering temperatures the samples seemed to be porous.

3. Results and discussion

3.1. Thermal stability of $LaNi_xFe_{1-x}O_{3-\delta}$ ($x=1.0$, 0.9, 0.8, 0.7) phases in air

The temperature dependences of specific electrical conductivity obtained for the single phase $LaNi_xFe_{1-x}O_{3-\delta}$ solid solutions with $x=1.0$, 0.9, 0.8, 0.7 are presented in Fig. 1. It is suggested that the changes in monotonicity of each curve correspond to the beginning of perovskite phase decomposition.

Undoped lanthanum nickelate $LaNiO_{3-\delta}$ decomposes completely at fixed T and $p(O_2)$ forming $La_4Ni_3O_{10-\delta}$ and NiO, because this three-phase equilibrium is nonvariant [20,23]. An addition of one component (Fe) makes this three-phase system monovariant. Therefore, a decrease in oxygen pressure leads to changes in composition of coexisting oxides. From the general point of view decomposition process of solid solution at the limiting conditions (temperature and oxygen pressure) occurs as follows: the composition of solid solution is depleted in some components and additional phases, relatively enriched by those components, appear. As a rule, decomposition process of complex oxides containing 3*d*-transition metals (while temperature increases or oxygen pressure decreases) is accompanied by a decrease in oxidation state of these metals at least in one of the products.

XRD analysis of decomposed $LaNi_xFe_{1-x}O_{3-\delta}$ ($x<1$) samples showed the presence of the following phases: rhombohedral perovskite phase (sp.gr. $R-3c$), orthorhombic phase $La_4(Ni,Fe)_3O_{10-\delta}$ (sp.gr. *Cmcm*) and (Ni,Fe)O (sp.gr. *Fm*3*m*). Such a phase composition is in a good agreement with the phase diagram of the La–Fe–Ni–O system obtained earlier at 1100 °C in air [21]. It should be mentioned that XRD analysis gave a true qualitative phase composition of the samples after decomposition because they were cooled down at a cooling rate of 400°/h compared to a heating rate of 10°/h that prevented the possibility of reverse formation of perovskite phase during cooling process. Taking into account the results of XRD analysis the decomposition reaction of $LaNi_xFe_{1-x}O_{3-\delta}$ ($x=0.9$, 0.8, and 0.7) while temperature increase (or oxygen partial pressure decrease) can be written as follows:

$$LaNi_xFe_{1-x}O_{3-\delta} = aLaNi_yFe_{1-y}O_{3-\delta} + bLa_4(Ni_{1-z}Fe_z)_3O_{10-\delta} + b(Ni_{1-v}Fe_v)O + cO_2, \quad (1)$$

Here, $y<x$ and $(Ni_{1-v}Fe_v)O$ solid solution is enriched with nickel in comparison with the perovskite phases. In the other words, each limiting composition of $LaNi_xFe_{1-x}O_{3-\delta}$ corresponds to the particular fixed conditions (T, pO_2) and gradual changes in these conditions lead to a gradual change in the limiting composition of the solid solution.

The proposed decomposition mechanism for iron-substituted lanthanum nickelates $LaNi_xFe_{1-x}O_{3-\delta}$ is in a good agreement

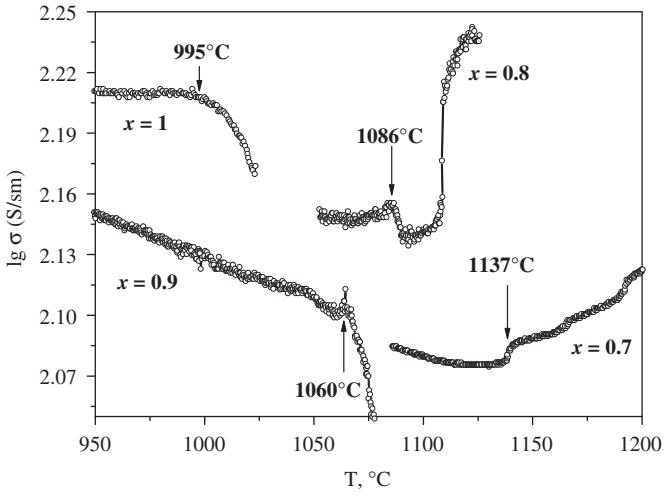

Fig. 1. Temperature dependences of the total conductivity of R-$LaNi_xFe_{1-x}O_{3-\delta}$ oxides (x=0.7–1.0).

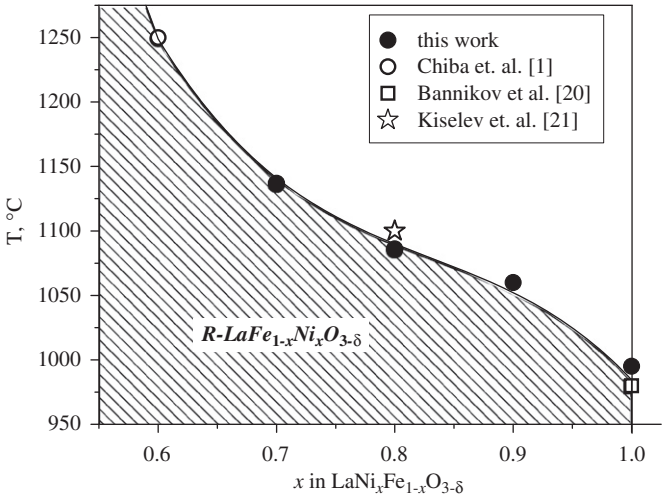

Fig. 2. Thermal stability of R-$LaNi_xFe_{1-x}O_{3-\delta}$ solid solutions in air.

with the thermal stability of lanthanum nickelates summarized in [23] and phase relations in the quasi-binary system $LaFeO_3$–"$LaNiO_{3-\delta}$", which will be discussed below.

The thermal stability of rhombohedral $LaNi_xFe_{1-x}O_{3-\delta}$ solid solutions significantly increases with iron content $(1-x)$ according to the results of the present study and earlier papers [1,20,21], which well agree with each other (Fig. 2).

3.2. Phase diagram of the quasi-binary $LaFeO_{3-\delta}$–"$LaNiO_{3-\delta}$" system

According to the result of XRD analysis two types of single-phase $LaFe_{1-x}Ni_xO_{3-\delta}$ oxides were obtained after equilibrating anneals at 1100 °C in air: with orthorhombic perovskite structure (sp.gr. *Pbnm*) within the range x=0.1–0.4 and with rhombohedral perovskite structure (sp.gr. $R-3c$) for the samples with x=0.6 and 0.7. The sample with nominal composition $LaFe_{0.5}Ni_{0.5}O_{3-\delta}$ consisted of two above-mentioned orthorhombic and rhombohedral perovskite phases with limiting compositions (x close to 0.4 and 0.6, respectively). XRD pattern of the $LaFe_{0.2}Ni_{0.8}O_{3-\delta}$ sample revealed reflections of the rhombohedral perovskite (sp.gr. $R-3c$) as a major phase and $La_4(Ni,Fe)_3O_{10}$ (~1%) as an impurity.

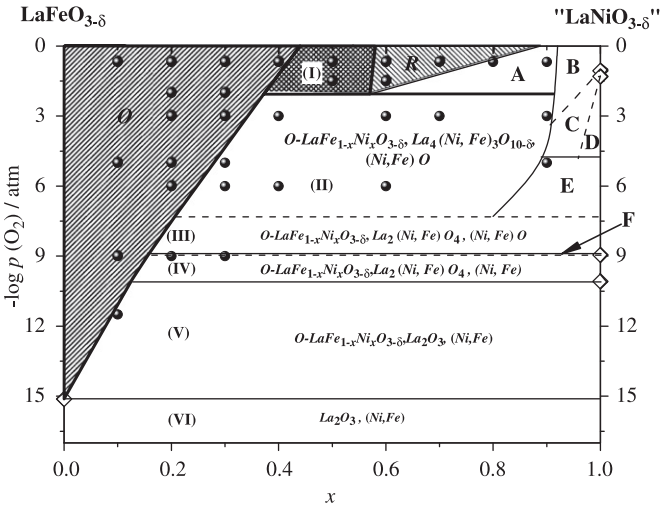

Fig. 3. Isothermal $LaFeO_{3-\delta}$–"$LaNiO_{3-\delta}$" cross-section of the phase diagram of the La–Ni–Fe–O system at 1100 °C. O and R denote $LaFe_{1-x}Ni_xO_{3-\delta}$ solid solutions with orthorhombically ($x \le 0.4$) and rhombohedrally distorted perovskite structure ($0.6 \le x < 0.8$), respectively. The phase composition of other fields that do not specified in the diagram are: (A) R-$LaFe_{1-x}Ni_xO_{3-\delta}$, $La_4(Ni,Fe)_3O_{10-\delta}$, (Ni,Fe)O; (B) $La_4(Ni,Fe)_3O_{10-\delta}$, (Ni,Fe)O; (C) $La_4(Ni,Fe)_3O_{10-\delta}$, $La_3(Ni,Fe)_2O_{7-\delta}$, (Ni,Fe)O; (D) $La_3(Ni,Fe)_2O_{7-\delta}$, $La_2(Ni,Fe)O_{4+\delta}$, (Ni,Fe)O; (E) $La_4(Ni,Fe)_3O_{10-\delta}$, $La_2(Ni,Fe)O_{4+\delta}$, (Ni,Fe)O; (F) O-$LaFe_{1-x}Ni_xO_{3-\delta}$, $La_2(Ni,Fe)O_{4+\delta}$, (Ni,Fe)O, (Ni,Fe) alloy.

The observed phase relations for $LaFe_{1-x}Ni_xO_{3-\delta}$ series are in a good agreement with the ones reported previously [21] except for $LaFe_{0.2}Ni_{0.8}O_{3-\delta}$ (single phase in [21] and ~1% of impurity in the present study). This slight discrepancy is probably caused by more precise XRD used in the present work or due to the deviations in the temperature control during the annealing of the samples in earlier work [21]. Furthermore, in the previous section, it was shown that $LaFe_{0.2}Ni_{0.8}O_{3-\delta}$ sample started to decompose at temperature about 1086 °C in air.

The phase composition of the $LaFe_{1-x}Ni_xO_{3-\delta}$ samples, quenched at various oxygen partial pressures from 1100 °C to room temperature, was determined by XRD. Overall compositions of the samples annealed at particular oxygen pressure $p(O_2)$ are shown as filled circles in the isothermal $LaFeO_{3-\delta}$–"$LaNiO_{3-\delta}$" cross-section of phase diagram of the La–Fe–Ni–O system (Fig. 3).

Phase relations in the La–Fe–Ni–O system can be represented in different diagram forms. If both temperature and oxygen pressure are fixed a phase diagram can be shown as compositional tetrahedron. However, if we like to use oxygen pressure as a variable it is better to represent the composition of condensed phases in the form of triangle based on the metallic components joint with $p(O_2)$ axis in perpendicular direction [24]. Oxygen content of each phase cannot be determined from this form of diagram but can be presented as assigned value. Since the total composition of each studied sample obey the ratio La:(Fe+Ni)=1:1, suggested phase diagram in the form of triangle prism can be presented as its plane $LaFeO_{3-\delta}$–"$LaNiO_{3-\delta}$" cross-section. It has to be noted that not all fields of obtained cross-section represent coexisting phases lying in this particular plane. Most of them are just cross-sections of the polyhedrons based on the phases located beyond the presented plane within three-dimensional La–Fe–Ni–O phase diagram. Since $LaNiO_{3-\delta}$ is not stable at 1100 °C within the whole range of studied $p(O_2)$, all fields in the cross-section (Fig. 3), adjoining to the right-hand axis (corresponded to the nominal composition "$LaNiO_{3-\delta}$"), are of that type.

As can be seen from Fig. 3, the $p(O_2)$-stability range both of orthorhombic (O) and rhombohedral (R) solid solutions is

enlarged with decreasing the nickel concentration (x) in $LaFe_{1-x}Ni_xO_{3-\delta}$ as expected from the $p(O_2)$–T-stability range of the parent oxides $LaFeO_{3-\delta}$ [18,25] and $LaNiO_{3-\delta}$ [19,20]. The boundary of existence for O-$LaFe_{1-x}Ni_xO_{3-\delta}$ varies from $x=0$ at $\log p(O_2)/\text{atm}=-15.12$ [25] to $x\sim0.4$ at $\log p(O_2)/\text{atm}=-0.68$ and that of for R-$LaFe_{1-x}Ni_xO_{3-\delta}$ is changed from $x\sim0.6$ at $\log p(O_2)/\text{atm}=-2.06$ to $x\sim0.8$ at $\log p(O_2)/\text{atm}=-0.68$. Therefore the two-phase field (I), consisting of both orthorhombic (near $x=0.4$) and rhombohedral (near $x=0.6$) $LaFe_{1-x}Ni_xO_{3-\delta}$ perovskites, is limited by the boundary of existence for the later composition. The phase composition of the fields O, R, and (I) and their boundaries listed above was confirmed by XRD. Some of the Rietveld-refined XRD patterns of the $LaFe_{1-x}Ni_xO_{3-\delta}$ samples with nominal compositions $x=0.1$, 0.2, 0.4, 0.6 annealed at 1100 °C under various $p(O_2)$ and then quenched to room temperature are shown in Fig. 4. The border of existence of O-$LaFe_{1-x}Ni_xO_{3-\delta}$ phases was also evaluated on the basis of refined unit cell parameters of coexisting phases performed for multi-phase samples from the field **(II)** (Fig. 4).

The phase composition of the B, C, D and E fields, which do not contain perovskite phases was deduced from the stability limits of undoped lanthanum nickelates $La_4Ni_3O_{10-\delta}$ and $La_3Ni_2O_{7-\delta}$ [23] (represented as open rhombs on the right-hand axis in Fig. 3), homogeneity ranges of $La_4(Ni_{1-y}Fe_y)_3O_{10-\delta}$ ($0\le y\le0.3$), $La_3(Ni_{1-z}Fe_z)_2O_{7-\delta}$ ($0\le z\le0.05$) and $Ni_{1-m}Fe_mO$ ($0\le m\le0.05$) solid solutions in air [21], and observed phase composition of experimental points from the fields A, E and **(II)**. All the samples with compositions inside the field **(II)** contain O-$LaFe_{1-x}Ni_xO_{3-\delta}$ perovskite, orthorhombic phases with the general formula $La_4(Ni,Fe)_3O_{10-\delta}$ (sp.gr. *Cmcm*), and cubic (Ni,Fe)O (sp.gr. *Fm*3*m*). For instance, Fig. 4 demonstrates the Rietveld-refined XRD patterns of the samples with nominal compositions $LaFe_{0.6}Ni_{0.4}O_{3-\delta}$ and $LaFe_{0.4}Ni_{0.6}O_{3-\delta}$, both annealed and then quenched in atmosphere with $p(O_2)=10^{-3}$ atm. The sample within the field E (Fig. 3) contains three phases in equilibrium: (Ni,Fe)O (sp.gr. *Fm*3*m*), $La_4(Ni,Fe)_3O_{10-\delta}$ (sp.gr. *Cmcm*) and a trace amount of tetragonal phase $La_2(Ni,Fe)O_{4+\delta}$ (sp.gr. *I*4/*mmm*).

The boundary lines between the C and D, C and E, E and D fields in the $LaFeO_{3-\delta}$–"$LaNiO_{3-\delta}$" cross-section are drawn schematically since they have to be presented in the diagram due to the existence of $La_3(Ni,Fe)_2O_{7-\delta}$ solid solution [21]. The uncertainty of the dash line separating the field E and **(III)** (Fig. 3) is caused by the lack of experimental data on $p(O_2)$-stability of $La_4(Ni,Fe)_3O_{10-\delta}$ solid solution. For that reason it is also drawn schematically in between of obtained experimental points. It should be noted that since the phases in which the ratio

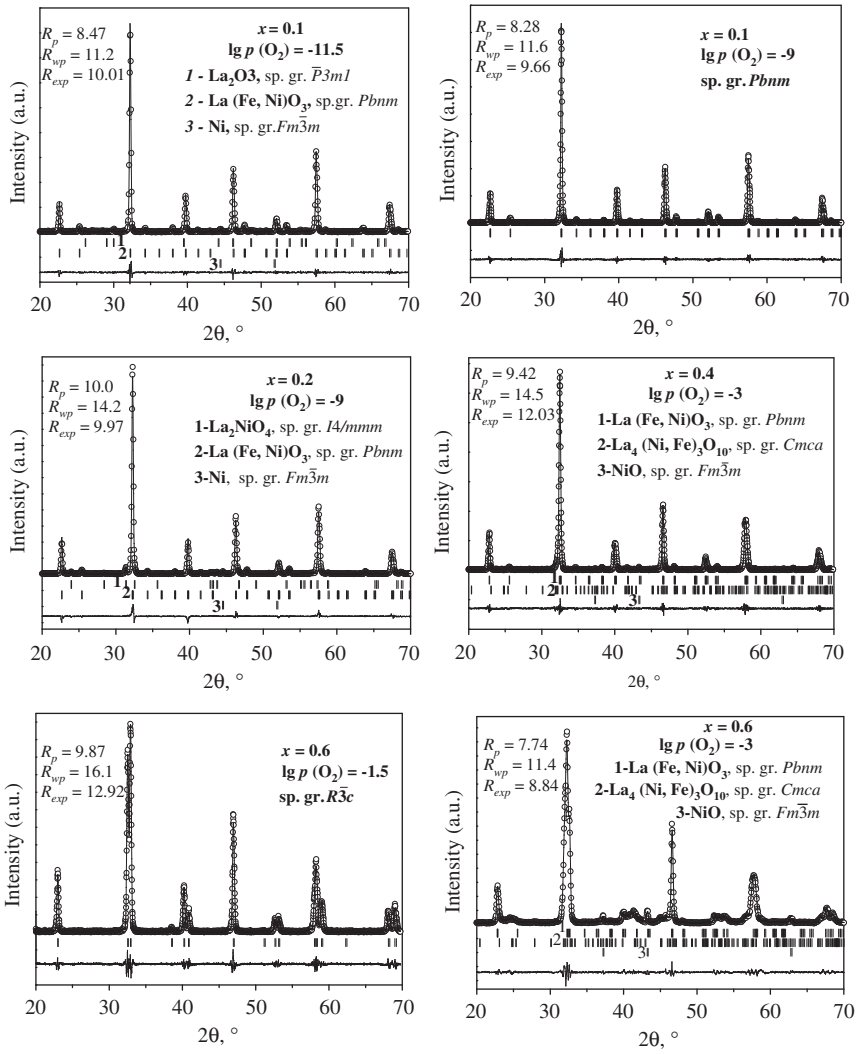

Fig. 4. XRD patterns of the $LaFe_{1-x}Ni_xO_{3-\delta}$ ($x=0.1$, 0.2, 0.4 and 0.6) samples annealed at 1100 °C under various $p(O_2)$ and quenched to room temperature. Open circles denote experimental points; upper solid lines are calculated profiles. Theoretical peak positions (vertical sticks) and difference lines are shown in the bottom of each pattern.

$n_{La}:n_{(Ni+Fe)} \neq 1:1$ do not belong to the plane of selected cross-section their compositions (Fe/Ni ratio) should not be determined from the presented phase diagram fragment (Fig. 3).

Special attention should be paid to the field *F* similarly to the fields (III) and (IV) that contains coexisting perovskite-type and K_2NiF_4-type solid solutions. This field represents the equilibrium transformation described by the following reaction:

$$(Ni_{1-v}Fe_v)O \Leftrightarrow a(Ni_{1-v'}Fe_{v'})O + b(Ni_{1-k}Fe_k) + cO_2. \quad (2)$$

The width of this field is very narrow, but the phase equilibria in the Fe–Ni–O system within the Ni-enriched range of compositions [26] prove its existence.

The boundaries between the fields (IV)–(V) and the fields (V)–(VI) at $\log p(O_2) = -10.05$ and $\log p(O_2) = -15.12$ in the $LaFeO_{3-\delta}$–"$LaNiO_{3-\delta}$" cross-section represent the La_2NiO_4/La_2O_3, Ni [24] and $LaFeO_3/La_2O_3$, Fe [25] equilibria, respectively. Since the fraction of iron in the $La_2(Ni,Fe)O_{4+\delta}$ solid solution does not exceed 0.075 in air [21] we suppose that the decomposition pressure $p(O_2)$ of limiting solid solution is practically the same (horizontal line at $\log p(O_2) = -10.05$ in Fig. 3) as for undoped La_2NiO_4.

The Rietveld analysis of XRD data for single-phase *O*-$LaFe_{1-x}Ni_xO_{3-\delta}$ allowed us to evaluate the effect of decreasing $p(O_2)$ on the values of refined unit cell parameters. The obtained $\log p(O_2)$-dependences of the unit cell parameters for single-phase *O*-$LaFe_{1-x}Ni_xO_{3-\delta}$ samples with $x = 0.1$, 0.2 and 0.3 annealed at 1100 °C and quenched to room temperature are shown in Fig. 5. The unit cell parameters increase when $p(O_2)$ decreases at a given *x*, as expected. Such behavior can be related to the lowering of oxygen content $(3-\delta)$ that consequently leads to a decrease in average oxidation state of 3*d*-transition metals (Fe,Ni) in the *O*-$LaFe_{1-x}Ni_xO_{3-\delta}$ oxide. It becomes obvious if one compares the effective ionic radii of 3*d*-metals in different oxidation states (CN=6): $r(Fe^{4+}) = 0.585$ Å $< r(Fe^{3+}) = 0.645$ Å $< r(Fe^{2+}) = 0.78$ and $r(Ni^{3+}) = 0.56$ Å $< r(Ni^{2+}) = 0.69$ Å [27]. This effect is well known as isothermal, or chemical, or, in other words, defect-induced expansion [28–32]. The dependences of the unit cell parameters versus composition (*x*) at fixed $p(O_2)$ for *O*-$LaFe_{1-x}Ni_xO_{3-\delta}$ can be also explained based on a size factor since the effective ionic radii of iron are larger than those of nickel in the same oxidation state: $r(Fe^{3+}) = 0.645$ Å $> r(Ni^{3+}) = 0.56$ Å and $r(Fe^{2+}) = 0.78 > r(Ni^{2+}) = 0.69$ Å [27]. A similar dependence of the unit cell parameters versus composition was observed earlier [14,16,21] for $LaFe_{1-x}Ni_xO_{3-\delta}$ synthesized at $p(O_2) = 0.21$ atm.

4. Conclusion

The $p(O_2)$-stability of the perovskite phases $LaFe_{1-x}Ni_xO_{3-\delta}$ has been evaluated at 1100 °C based on XRD analysis of powder samples annealed under various $p(O_2)$ and quenched to room temperature. The isothermal $LaFeO_{3-\delta}$–"$LaNiO_{3-\delta}$" cross-section of the phase diagram of the La–Fe–Ni–O system has been proposed within the range of oxygen partial pressure $-15 < \log p(O_2)/\text{atm} \leq -0.68$. It has been shown that the unit cell parameters of the orthorhombic perovskites *O*-$LaFe_{1-x}Ni_xO_{3-\delta}$ increase with decrease in $p(O_2)$ at a given *x*. The decomposition temperatures of rhombohedral phases *R*-$LaFe_{1-x}Ni_xO_{3-\delta}$ for

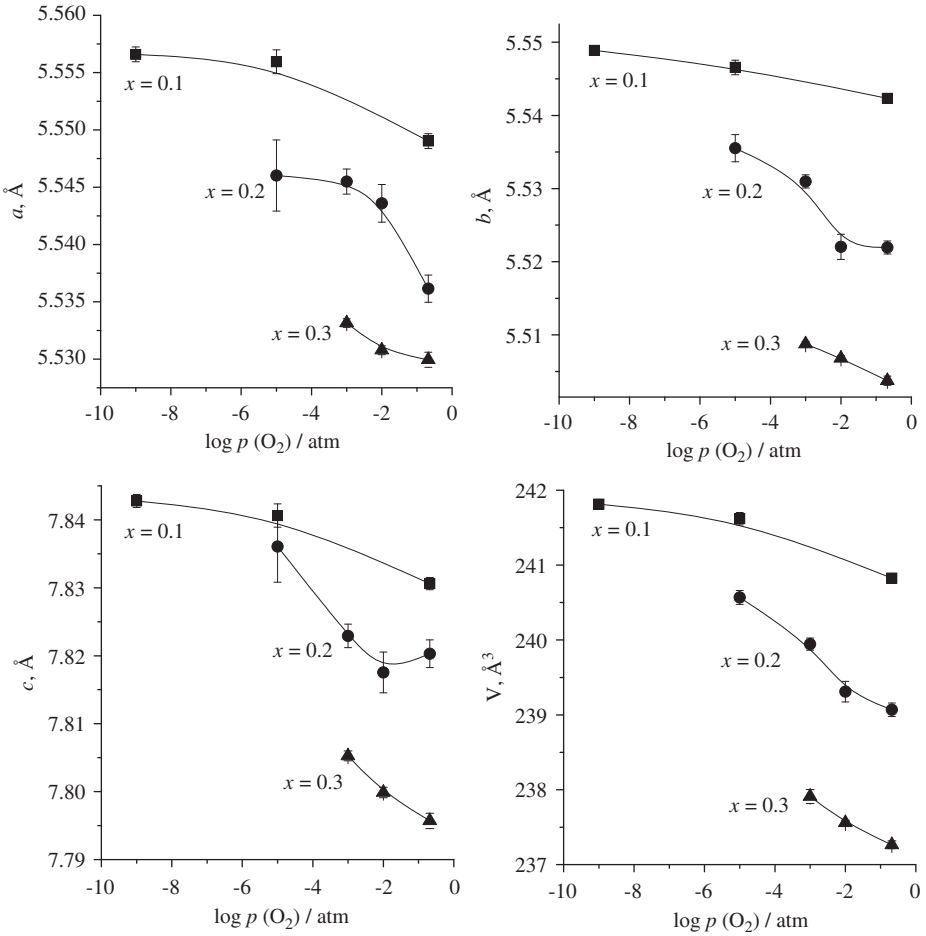

Fig. 5. Log $p(O_2)$-dependences of unit cell parameters for *O*-$LaFe_{1-x}Ni_xO_{3-\delta}$ oxides annealed at 1100 °C under various $p(O_2)$ and quenched to room temperature.

$x=0.7$, 0.8, 0.9 and 1.0 in air were determined as 1137, 1086, 1060 and 995 °C, respectively.

Acknowledgments

This work was financially supported in parts by the Russian Foundation for Basic Research (Project no. 09-03-00620) and Ministry of Education and Science of the Russian Federation. Experimental assistance made by A.A. Raskovalov is gratefully acknowledged.

References

[1] R. Chiba, F. Yoshimura, Y. Sakurai, Solid State Ionics 124 (1999) 281–288.
[2] R.N. Basu, F. Tietz, O. Teller, E. Wessel, H.P. Buchkremer, D. Stover, J. Solid State Electrochem. 7 (2003) 416–420.
[3] S.M. Lima, J.M. Assaf, Mater. Res. 5 (2002) 329–335.
[4] R. Chiba, Y. Tabata, T. Komatsu, H. Orui, K. Nozawa, M. Arakawa, H. Arai, Solid State Ionics 78 (2008) 1701–1709.
[5] T. Komatsu, R. Chiba, H. Arai, K. Sato, J. Power Sources 176 (2008) 132–137.
[6] M.D. Mat, X. Liub, Zh. Zhuc, B. Zhu, Int. J. Hydrogen Energy 32 (2007) 796–801.
[7] S. Li, X. Sun, Zh. Wen, J. Sun, Rare Met. 25 (2006) 213–217.
[8] R.N. Basu, F. Tietz, E. Wessel, D. Stöver, J. Mat., Proc. Tech. 147 (2004) 85–89.
[9] K. Świerczek, J. Marzec, D. Pałubiak, W. Zając, J. Molenda, Solid State Ionics 177 (2006) 1811–1817.
[10] W. Zając, K. Swierczek, J. Molenda, J. Power Sources 173 (2007) 675–680.
[11] M. Bevilacqua, T. Montini, C. Tavagnacco, E. Fonda, P. Fornasiero, M. Graziani, Chem. Mater. 19 (2007) 5926–5936.
[12] K. Iwasaki, T. Ito, M. Yoshino, T. Matsui, T. Nagasaki, Yu. Arita, J. Alloys Compd. 430 (2007) 297–301.
[13] R. Funahashi, M. Mikami, S. Urata, M. Kitawaki, T. Kouuchi, K. Mizuno, Meas. Sci. Technol. 16 (2005) 70–80.
[14] H. Falcon, A.E. Goeta, G. Punte, R.E. Carbonio, J. Solid State Chem. 133 (1997) 379–385.
[15] V.V. Kharton, A.P. Viskup, E.N. Naumovich, V.N. Tikhonovich, Mater. Res. Bull. 34 (1999) 1311–1317.
[16] N.V. Proskurnina, V.I. Voronin, V.A. Cherepanov, E.A. Kiselev, Prog. Solid State Chem. 35 (2007) 233–239.
[17] M. Gateshki, L. Suescun, S. Kolesnik, J. Mais, K. Swierczek, S. Short, B. Dabrowski, J. Solid State Chem. 181 (2008) 1833–1839.
[18] V.L. Moruzzi, M.W. Shafer, J. Am. Ceram. Soc. 43 (1960) 367–372.
[19] T. Nakamura, G. Petzow, L.J. Gauckler, Mater. Res. Bull. 14 (1979) 649–659.
[20] D.O. Bannikov, V.A. Cherepanov, J. Solid State Chem. 179 (2006) 2721–2727.
[21] E.A. Kiselev, N.V. Proskurnina, V.I. Voronin, V.A. Cherepanov, Inorg. Mater. 43 (2007) 167.
[22] J. Rodriguez-Carvajal, Physica B 192 (1993) 55–69.
[23] M. Zinkevich, F. Aldinger, J. Alloys Compd. 375 (2004) 147–161.
[24] A.N. Petrov, V.A. Cherepanov, A.Y.u Zuev, V.M. Zhukovsky, J. Solid State Chem. 77 (1988) 1–14.
[25] N. Kimizuka, A. Yamamoto, H. Ohashi, T. Sugihara, T. Sekine, J. Solid State Chem. 49 (1983) 65–76.
[26] F. Schneider, H. Schmalzried, Z. Phys. Chem. NF 166 (1990) 1.
[27] R.D. Shannon, Acta Crystallogr. A: Cryst. Phys. Diffr. Theor. Gen. Crystallogr. 32 (1976) 751–767.
[28] T.R. Armstrong, J.W. Stevenson, L.R. Pederson, P.E. Raney, J. Electrochem. Soc. 143 (1996) 2919–2925.
[29] P.H. Larsen, P.V. Hendriksen, M. Mogensen, J. Therm. Anal. 49 (1997) 1263–1275.
[30] A. Zuev, L. Singheiser, K. Hilpert, Solid State Ionics 147 (2002) 1–11.
[31] K. Hilpert, R.W. Steinbrech, F. Boroomand, E. Wessel, F. Meschke, A. Zuev, O. Teller, H. Nickel, L. Singheiser, J. Eur. Ceram. Soc. 23 (2003) 3009–3020.
[32] A.Y.u Zuev, A.I. Vylkov, A.N. Petrov, D.S. Tsvetkov, Solid State Ionics 179 (2008) 1876–1879.